Int J Fract (2010) 161:21–39
DOI 10.1007/s10704-009-9423-7

ORIGINAL PAPER

Dynamic crack propagation analysis of orthotropic media by the extended finite element method

D. Motamedi · S. Mohammadi

Received: 5 April 2009 / Accepted: 26 October 2009 / Published online: 24 November 2009

Abstract Dynamic crack propagation of composites is investigated in this paper based on the recent advances and development of orthotropic enrichment functions within the framework of partition of unity and the extended finite element method (XFEM). The method allows for analysis of the whole crack propagation pattern on an unaltered finite element mesh, defined independent of the existence of any predefined crack or its propagation path. A relatively simple, though efficient formulation is implemented, which consists of using a dynamic crack initiation toughness, a crack orientation along the maximum circumferential stress, and a simple equation to presume the crack speed. Dynamic stress intensity factors (DSIFs) are evaluated by means of the domain separation integral method. The governing elastodynamics equation is first transformed into a standard weak formulation and is then discretized into an XFEM system of time dependent equations, to be solved by the unconditionally stable Newmark time integration scheme. A number of benchmark and test problems are simulated and the results are compared with available reference results.

Keywords Extended finite element method (XFEM) · Crack propagation · Dynamic stress intensity factor · Composites

D. Motamedi · S. Mohammadi (✉)
School of Civil Engineering, University of Tehran, Tehran, Iran
e-mail: smoham@ut.ac.ir

1 Introduction

Rapid development in construction and application of composite materials in various ordinary and high tech engineering applications has resulted in extensive research work to enhance the computational efficiency of the existing methods or to the develop new ideas to analyse crack stability and propagation of composite structures. In these set of problems, crack initiation, propagation direction and crack tip state are usually the main concerns of simulation. Static and quasi-crack analyses have been widely used for fracture analysis of composites (Atluri et al. 1975; Forschi and Barret 1976; Boone et al. 1987). Nevertheless, they do not represent real world crack problems; they are only used as efficient simplified models for other highly complex dynamic phenomena.

Several numerical methods have been proposed in the last decades in order to predict and analyze cracking in composites. One of the well-known methods is the remeshing technique which adopts a discrete crack model for progressive crack propagation under quasi-static and dynamic loadings (Maigre and Rittel 1993; Combescure et al. 2008). This technique implements the simplicity of classical finite element method (FEM) with the sophistication of adaptive remeshing techniques in each time-step when the cracks propagate. Despite the fact that this method is fundamentally simple and is employed by a number of commercial finite element softwares, the method suffers from a number of drawbacks. First, it is time consuming and is not

suited to simulate problems with several cracks. Also, nodal alignments may cause numerical difficulties and mesh dependency in propagation problems. Finally, the continuum based finite element formulation is unable to reproduce the physical singular stress field at the tip of a crack.

In order to avoid such difficulties, new approaches, which avoid the implementation of new nodes, have been proposed by Xu and Needleman (1994) and Camacho and Ortiz (1996) through the cohesive segments. Alternatively, the basis of XFEM was introduced by Belytschko and Black (1999) and promoted by Moës et al. (1999). They implemented the concept of partition of unity (PUM), introduced earlier by Melenk and Babuška (1996), to develop a method to model discontinuity. Further investigations have subsequently been carried out; including Sukumar et al. (2000) and Areias and Belytschko (2005) extending the method to three dimensional domain, Dolbow et al. (2001) using frictional contact, Mergheim et al. (2005) simulating cohesive cracks and Belytschko et al. (Belytschko et al. 2003; Belytschko and Chen 2004) modeling dynamic crack propagation for isotropic materials.

Two independent parts are involved in a dynamic crack analysis by XFEM. First, a crack tracking procedure is required to represent an existing crack and its evolution by time. Fortunately, the level set method and the fast marching approach are available. They have been successfully implemented in the XFEM codes and can be used for quasi-static or dynamic crack evolution problems (Ventura et al. 2003).

The second part is related to the way dynamic crack propagation is formulated. Belytschko et al. (2003) developed a methodology for switching from a continuum to a discrete discontinuity where the governing partial differential equation loses hyperbolicity for rate independent materials. They adopted the technique of loss of hyperbolicity in combination with the XFEM cohesive crack models. The idea was to track the change of a hyperbolicity indicator to compute the direction and velocity of dynamic crack propagation. They applied the method to solve problems involving crack branching. The idea of loss of hyperbolicity was previously developed by Gao and Klein (1998) for analysing dynamic crack propagations. Later, Peerlings et al. (2002) and Oliver et al. (2003) further studied the loss of hyperbolicity and added this technique into equilibrium equations.

Further improvements were reported by Chessa and Belytschko (2004, 2006). They presented a locally enriched space–time extended finite element method for solving hyperbolic problems with discontinuities. The coupling was implemented through a weak enforcement of the continuity of the flux between the space–time and semi-discrete domains in a manner similar to discontinuous Galerkin methods. They successfully applied the TXFEM to the Rankine–Hugoniot jump conditions to linear first order wave and nonlinear Burgers equations.

Furthermore, Réthoré et al. (2005) proposed a combined space–time extended finite element method, based on the idea of the time extended finite element method (TXFEM), allowing a suitable form of the time stepping formulae to satisfy stability and energy conservation criteria. XFEM was used to implicitly define a virtual crack field tangential to the crack front. The concept of a virtual field allowed for separation of mixed modes of fracture.

Other contributions include the work by Belytschko and Chen (2004) who developed a singular enrichment finite element method for elastodynamic crack propagation, Zi et al. (2005) who presented a method for modelling arbitrary growth of dynamic cracks without remeshing, and Menouillard et al. (2006) who introduced a lumped mass matrix for enriched elements, which allowed the use of a pure explicit formulation in XFEM applications.

In this study, orthotropic enrichment functions, recently proposed by Asadpoure et al. (2006a,b), Asadpoure and Mohammadi (2007), and Mohammadi (2008), are extended to dynamic problems to simulate dynamic crack propagation with XFEM. By this means, the displacement and stress fields near a crack tip are expected to be accurately approximated. This is achieved by modification of the very basic linear static FE interpolation $\left(u^h(x) = \sum N_i u_i\right)$ into a new enriched approximation to resemble the singularity nature of stress field near crack tips within orthotropic media. Other issues such as boundary conditions, dynamic effects, etc. will be automatically handled by the dynamic finite element analysis using a proper time integration scheme. The present approach is expected to improve orthotropic elastodynamic crack analyses even by modification of the basic elastostatic approximation of the finite element interpolation around a crack tip. A similar approach has recently been adopted by Réthoré et al. (2005) and Combescure et al. (2008)

to model the dynamic crack propagation in isotropic media using static isotropic enrichment functions.

In the first section of this paper, the basic formulations of fracture mechanics of dynamic crack propagation in orthotropic media are introduced. Furthermore, the idea of separation integral domain for evaluation of the dynamic stress intensity factors through J integral is explained. Then, implementation of XFEM in modeling dynamic crack propagation has described. Finally, in order to verify the proposed formulation and to investigate its robustness, the dynamic stress intensity factors (DSIFs) are compared with other available data in a set of numerical problems.

2 Dynamic fracture mechanics

2.1 Dynamic fracture laws

The crack propagation law should be chosen based upon the type of material which is being simulated or experimented. Despite the fact that simulation of dynamic brittle crack propagation remains a difficult challenge, the physical modeling of fracture phenomenon is comprised of relatively three simple concepts (Gregoire et al. 2007):

(1) a criterion is required to describe the stability/instability of an existing crack;
(2) an equation is needed in order to find the propagation direction, if the crack becomes unstable;
(3) an equation to specify the crack propagation speed.

In this study, the stress intensity factor is compared with the dynamic crack initiation toughness to evaluate the crack instability. The dynamic crack initiation toughness is a material property and can be obtained by experiment. If the crack violates such a stability criterion, it starts to propagate and the direction of propagation is that of the maximum hoop stress (Maigre and Rittel 1993). An implicit approach, which updates the crack-tip new position at the end of each step, is adopted to calculate the crack extension. Using the crack propagation direction, K^* is calculated and the crack-tip velocity is obtained. Then, in each step, the crack growth is calculated by multiplying the size of the time step and the ratio of current and previous crack velocities.

During the crack propagation, the crack speed adapts its value in a way to make the maximum hoop stress intensity factor become equal to the dynamic crack growth toughness. To evaluate the dynamic crack growth toughness, Kanninen and Popelar (1985) proposed to replace the quasi-static toughness by the dynamic crack initiation toughness. In this method, the dynamic crack growth toughness is considered to be (Gregoire et al. 2007):

$$\begin{aligned} &K^* < K_{1d} \quad (no\ initiation)\\ &K^* = K_{1d},\ \theta^* = \theta_c \quad (initiation)\\ &K^*(t,v) \geq K_{1d}(v) \Rightarrow K^*(t,v)\\ &\qquad = K_{1D}(v) \quad (propagation) \end{aligned} \tag{1}$$

where K^* is the dynamic maximum hoop stress intensity factor, K_{1d} is the dynamic crack initiation toughness, K_{1D} is the dynamic crack growth toughness and v is the crack growth speed, which can be elicited from the following equation (Gregoire et al. 2007):

$$v = C_R\left(1 - \frac{K_{1d}}{K^*}\right) \tag{2}$$

where C_R is the Rayleigh wave speed. In orthotropic materials, the Rayleigh wave speed is replaced with the shear wave speed C_S in Eq. 2. The maximum positive hoop stress can be calculated from (Aliabadia and Sollero 1998):

$$\begin{aligned} \sigma_{\theta\theta} = &\left\{ K_I \mathrm{Re}\left[\frac{\mu_1\mu_2\left(\frac{\mu_2}{B} - \frac{\mu_1}{A}\right)}{\mu_1 - \mu_2}\right] \right.\\ &\left. + K_{II}\mathrm{Re}\left[\frac{\frac{\mu_2^2}{B} - \frac{\mu_1^2}{A}}{\mu_1 - \mu_2}\right]\right\} \sin^2\theta\\ &+ \left\{ K_I \mathrm{Re}\left[\frac{\frac{\mu_1}{B} - \frac{\mu_2}{A}}{\mu_1 - \mu_2}\right] \right.\\ &\left. + K_{II}\mathrm{Re}\left[\frac{\frac{1}{B} - \frac{1}{A}}{\mu_1 - \mu_2}\right]\right\} \cos^2\theta\\ &- \left\{ K_I \mathrm{Re}\left[\frac{\mu_1\mu_2\left(\frac{1}{A} - \frac{1}{B}\right)}{\mu_1 - \mu_2}\right] \right.\\ &\left. + K_{II}\mathrm{Re}\left[\frac{\frac{\mu_1}{A} - \frac{\mu_2}{B}}{\mu_1 - \mu_2}\right]\right\} \sin 2\theta \end{aligned} \tag{3}$$

where K_I, K_{II} are the stress intensity factors and μ_1 and μ_2 are the complex roots (not conjugated pair) of following equation (Lekhnitskii 1963):

$$\begin{aligned} &a_{11}\mu^4 - 2a_{16}\mu^3 + (2a_{12} + a_{66})\,\mu^2\\ &-2a_{26}\mu + a_{22} = 0 \end{aligned} \tag{4}$$

where a_{ij} are the components of the compliance tensor ($\varepsilon = a_{ij}\sigma$). A and B are also defined as (Aliabadia and Sollero 1998):

$$A = \sqrt{(\cos\theta + \mu_1 \sin\theta)}$$
$$B = \sqrt{(\cos\theta + \mu_2 \sin\theta)} \quad (5)$$

The maximum hoop stress direction θ^* can be calculated by finding the extreme values of Eq. 3. The corresponding maximum hoop stress intensity factor can then be obtained from (Gregoire et al. 2007):

$$K^* = \cos^3\left(\frac{\theta^*}{2}\right) \quad K_I - \frac{3}{2}\sin\left(\theta^*\right)\cos\left(\frac{\theta^*}{2}\right) \quad K_{II} \quad (6)$$

In the present study, the material behavior is further idealized in order to simplify the process of crack modeling; the fiber composite structure is assumed as a homogeneous orthotropic continuum, where the crack growth takes place in an idealized material with anisotropic constituents. In this approach, the details of local failures of composite, such as broken fibers or cracked matrix, are not consider and an equivalent orthotropic continuum is adopted.

2.2 Dynamic stress intensity factors

Dynamic stress intensity factors, which play an important role in dynamic fracture problems, are used to calculate the positive maximum hoop stress intensity factor and to evaluate dynamic crack propagation properties.

In order to find dynamic stress intensity factors, the method proposed by Nishioka and Alturi (1984) is adopted. Accordingly, the analytical form of the dynamic J-integral (J_k') can be written as:

$$J_k' = \int_{\Gamma+\Gamma_c} \left((W+K)n_k - t_i \frac{\partial u_j}{\partial x_k}\right) d\Gamma + \int_{V_\Gamma - V_\varepsilon} \left((\rho\ddot{u}_i - f_i)\frac{\partial u_i}{\partial x_k} - \rho\frac{\partial \dot{u}_i}{\partial x_k}\dot{u}_i\right) dA \quad (7)$$

where u_i, t_i, f_i, n_k and ρ denote the displacement, traction, body force, outward normal direction, and mass density, respectively, $W = (1/2)\,\sigma_{ij}\varepsilon_{ij}$is the strain energy density, $K = (1/2)\rho\dot{u}_i\dot{u}_i$ is the kinetic energy density and the integral paths are defined in Fig. 1. Γ_ε, Γ, and Γ_c denote near-field, far-field and crack surface paths, respectively. V_Γ is the region encircled by

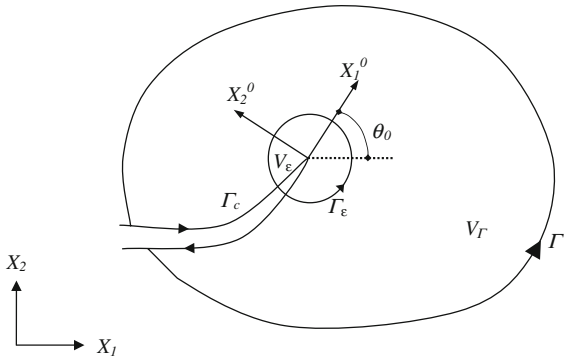

Fig. 1 Local crack-tip co-ordinates and the contour Γ and its interior area, V_Γ

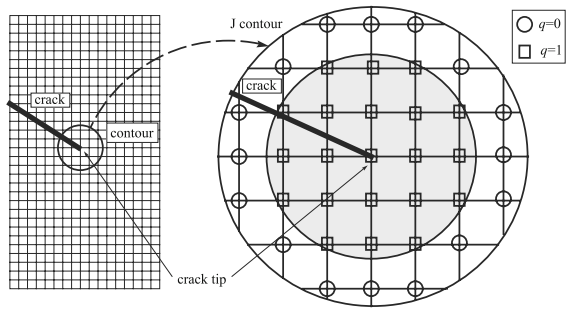

Fig. 2 Nodal value for function q

Γ, while V_ε represents the region surrounded by Γ_ε (Fig. 1). Inasmuch as the form of the first term of Eq. 7 is not well-suited for the finite element method, an equivalent form of Eq. 7 can be achieved by using the divergence theorem and some additional assumptions for homogeneous materials, as discussed by Kim and Paulino (2003),

$$J_k' = \int_{V_\Gamma} \left(\sigma_{ij}\frac{\partial u_j}{\partial x_k} - (W+K)\right) q_{,k}\, dA + \int_{V_\Gamma} \left((\rho\ddot{u}_i - f_i)\frac{\partial u_i}{\partial x_k} - \rho\frac{\partial \dot{u}_i}{\partial x_k}\dot{u}_i\right) q\, dA \quad (8)$$

where q is a function smoothly changing from $q = 1$ near a crack-tip to $q = 0$ at the exterior boundary, Γ. In the present study, q is assumed to be varying linearly from 1 to 0, as depicted in Fig. 2. Noting that the value of q is constant near the crack-tip area, distinguishable by shaded unaffected elements in Fig. 2, the gradient of q vanishes in Eq. 8.

The interaction integral method is frequently adopted in elastostactic crack analyses to evaluate mixed mode J integral and associated stress intensity factors.

Despite its more precise solution for static problems, another method based on the concept of dynamic energy release rate G is used in this work. To explain the reason, it is well known that the interaction integral method, requires several auxiliary field components to be computed. Therefore, equations of dynamic near-tip displacement and stress fields in orthotropic materials have to be derived in order to extract the required auxiliary displacement and stress fields. Moreover, more complex computations are required to calculate 'auxiliary velocity' and 'auxiliary strain velocity' fields. These required a substantial theoretical and simulation experience and cost (if possible at all). This might be the reason why most of the researches on dynamic behavior of materials using the interaction integral have been within the framework of isotropic media. On the other hand, an additional relation is required in orthotropic media under mixed mode dynamic conditions. Therefore, in the absence of access to all required elements for that approach in orthotropic materials, the present formulation based on G is preferred.

The crack-axis components of the dynamic J integral can be evaluated by the following coordinate transformation (Kim and Paulino 2003):

$$J_l'^0 = \alpha_{lk}(\theta_0) J_k' \tag{9}$$

where α_{lk} is the coordinate transformation tensor and θ_0 is the crack angle. The tangential component of the dynamic J integral, $J_l'^0$, corresponds to the rate of change in the potential energy per unit crack extension, namely, the dynamic energy release rate (G). Wu (2000) showed that the dynamic energy release rate can be related to the instantaneous stress intensity factors for an elasto-dynamically propagating crack with the speed v:

$$G = J_l'^0 = J_1' \cos\theta_0 + J_2' \sin\theta_0 \tag{10}$$

$$G = (1/2) K^T L^{-1}(v) K \tag{11}$$

where $L(v)$ has been presented by Dongye and Ting (1989), for orthotropic materials with the symmetry planes coinciding with the coordinate planes. The non-zero components of $L(v)$ are:

$$L_{33}(v) = \sqrt{\hat{C}_{55} C_{44}} \tag{12}$$

$$\sqrt{\hat{C}_{66} C_{22}} \quad L_{11}(v) = \sqrt{\hat{C}_{11} C_{66}} \quad L_{22}(v) = \Omega \Psi^{-\frac{1}{2}} \tag{13}$$

where $\hat{C}_{ij} = C_{ij} - \rho v^2 \delta_{ij}$, C_{ij} are the constitutive coefficients, ρ is the material density and

$$\Omega = \left(\hat{C}_{11} C_{22} - C_{12}^2\right) \sqrt{\hat{C}_{66} C_{66}} - \rho v^2 C_{66} \sqrt{\hat{C}_{11} C_{22}} \tag{14}$$

$$\Psi = \left(\sqrt{\hat{C}_{66} C_{66}} + \sqrt{\hat{C}_{11} C_{22}}\right)^2 - (C_{12} + C_{66})^2 \tag{15}$$

To accurately evaluate the in-plane mixed-mode stress intensity factors from the dynamic J integral, the component separation method, proposed by Aliabadia and Sollero (1998), is implemented. Aliabadia and Sollero (1998) discussed that the following relationship between the dynamic stress intensity factors and the relative sliding and opening displacements of the crack face can be obtained:

$$\begin{Bmatrix} \delta_1 \\ \delta_2 \end{Bmatrix} = \sqrt{\left(\frac{8r}{\pi}\right)} \begin{bmatrix} D_{11} & D_{12} \\ D_{21} & D_{22} \end{bmatrix} \begin{Bmatrix} K_I \\ K_{II} \end{Bmatrix} \tag{16}$$

with

$$D_{11} = Im\left(\frac{\mu_2 p_1 - \mu_1 p_2}{\mu_1 - \mu_2}\right), \quad D_{12} = Im\left(\frac{p_1 - p_2}{\mu_1 - \mu_2}\right)$$
$$D_{21} = Im\left(\frac{\mu_2 q_1 - \mu_1 q_2}{\mu_1 - \mu_2}\right), \quad D_{22} = Im\left(\frac{q_1 - q_2}{\mu_1 - \mu_2}\right) \tag{17}$$

where μ_k are defined in Eq. 4 and p_k and q_k are described below (Aliabadia and Sollero 1998):

$$p_k = a_{11}\mu_k^2 + a_{12} - a_{16}\mu_k \tag{18}$$

$$q_k = a_{12}\mu_k + \frac{a_{22}}{\mu_k} - a_{26} \tag{19}$$

The ratio of opening to sliding displacements, R_{COD}, can be written as:

$$R_{COD} = \frac{\delta_2}{\delta_1} = \frac{D_{21} K_I + D_{22} K_{II}}{D_{11} K_I + D_{12} K_{II}} \tag{20}$$

Therefore, the ratio of dynamic stress intensity factors, R_{SIF}, is obtained as:

$$R_{SIF} = \frac{K_I}{K_{II}} = \frac{R_{COD} D_{21} - D_{22}}{D_{21} + R_{COD} D_{11}} \tag{21}$$

Substitution for K_I from Eq. 21 into Eq. 20 leads to the following relationship for K_{II}:

$$K_{II} = \sqrt{\frac{2G}{L_{11}(v) RSIF^2 + L_{22}(v)}} \tag{22}$$

3 XFEM implementation of dynamic crack propagation

3.1 Basics of XFEM method

The extended finite element method was first introduced by Belytschko and Black (1999) in order to avoid explicit modeling of discrete cracks by enhancing the basic finite element solution through the use of enrichment functions. By implementing the generalized Heaviside function, proposed by Moës et al. (1999), the method was further enhanced, avoiding the need of complicated mapping for arbitrary curved cracks. Further general improvements have been made by Sukumar et al. (2000), Dolbow et al. (2001), Belytschko et al. (2003), Belytschko and Chen (2004), Asadpoure et al. (2006a,b), and Asadpoure and Mohammadi (2007), while specific extensions in field of dynamic crack propagation have recently been made by Gregoire et al. (2007) and Nistor et al. (2008). A general description and a comprehensive discussion on the method can be found in Mohammadi (2008).

In the extended finite element method, first, the finite element mesh is produced, regardless of the existence and location of any cracks. Afterwards, according to the location of any discontinuity, a few degrees of freedom are added to the classical finite element model in selected nodes around the discontinuity. They contribute to the approximation through the use of the generalized Heaviside and crack-tip (near-tip) functions. For modeling the crack propagation in each step, the crack growth is considered as straight segments. When an element is cut because of a crack growth, new Heaviside and singular enriched degree of freedoms will be added to the existing conventional degrees of freedom of the model (Gregoire et al. 2007).

Let's consider that there is a discontinuity within a domain which is already meshed into some elements with N nodes. The displacement field for a point x inside the domain, can be approximated based on the XFEM formulation proposed by Belytschko and Black (1999):

$$\mathbf{u}^g(\mathbf{x}) = \sum_{\substack{I \\ n_I \in \mathbf{N}}} \phi_I(\mathbf{x})\mathbf{u}_I + \sum_{\substack{J \\ n_J \in \mathbf{N}^f}} \phi_J(\mathbf{x})\psi(\mathbf{x})\mathbf{a}_J \qquad (23)$$

where n_I represents the node I, ϕ_I is the shape function associated with the node I, $\mathbf{u}_I$ is the FEM vector of regular degrees of freedom, $\mathbf{a}_J$ is the new set of enriched degrees of freedom added to the finite element degrees of freedom, $\mathbf{N}^f$ is the set of nodes that the discontinuity is in its influence (support) domain and $\psi(\mathbf{x})$ is the enrichment function (Fig. 3).

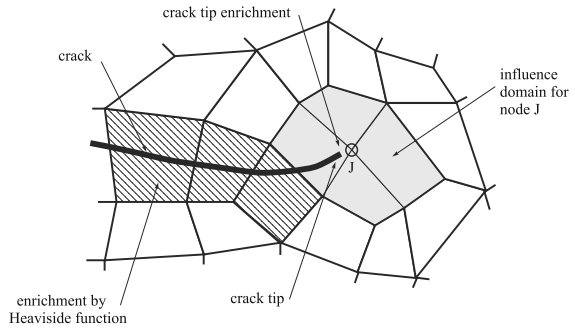

Fig. 3 Definition of the influence (support) domain for node J in an arbitrary finite element mesh

The first term in Eq. 23 is the classical finite element approximation to calculate the displacement field while the second term is the XFEM enriched displacement field related to the discontinuity.

In order to model crack edges and tips in the extended finite element, Moës et al. (1999) suggested that Eq. 23 can be generalized in the following form

$$\begin{aligned}\mathbf{u}^h(\mathbf{x}) = &\sum_{\substack{I \\ n_I \in \mathbf{N}}} \phi_I(\mathbf{x})\mathbf{u}_I + \sum_{\substack{J \\ n_J \in \mathbf{N}^g}} \mathbf{b}_J \phi_J(\mathbf{x}) H(\mathbf{x}) \\ &+ \sum_{k \in \mathbf{K}^1} \phi_k(\mathbf{x}) \left(\sum_l \mathbf{c}_k^{l1} F_l^1(\mathbf{x}) \right) \\ &+ \sum_{k \in \mathbf{K}^2} \phi_k(\mathbf{x}) \left(\sum_l \mathbf{c}_k^{l2} F_l^2(\mathbf{x}) \right) \end{aligned} \qquad (24)$$

where $\mathbf{N}^g$ is the set of nodes that their corresponded elements are cut by crack faces (but not crack-tip), $\mathbf{b}_J$ is the vector of additional degrees of freedom which are related to the modeling of crack faces (not crack-tips), $\mathbf{c}_k$ is the vector of additional degrees of freedom for modeling crack-tips, $F_l^i(\mathrm{x})$, $(i = 1, 2)$ are crack-tip enrichment functions and $\mathbf{K}^1$ and $\mathbf{K}^2$ are the sets of nodes associated with crack-tip 1 and 2 in their influence domain, respectively.

According to Moës et al. (1999), the Heaviside enrichment function is defined as:

$$H(\mathbf{x}) = \begin{cases} +1; & \text{if } (\mathbf{x} - \mathbf{x}^*) \cdot \mathbf{e_n} > 0 \\ -1; & \text{otherwise} \end{cases} \qquad (25)$$

In the present work, the following orthotropic enrichment functions, recently derived by Asadpoure and Mohammadi (2007) from the two-dimensional asymptotic displacement field near crack-tip in orthotropic materials, are implemented:

$$\{F_l(r,\theta)\}_{l=1}^{4} = \left\{\sqrt{r}\cos\frac{\theta_1}{2}\sqrt{g_1(\theta)}, \sqrt{r}\cos\frac{\theta_2}{2}\sqrt{g_2(\theta)}, \times \sqrt{r}\sin\frac{\theta_1}{2}\sqrt{g_1(\theta)}, \sqrt{r}\sin\frac{\theta_2}{2}\sqrt{g_2(\theta)}\right\} \quad (26)$$

which r and θ define the crack-tip based local polar coordinates of integral points, and $g_k(\theta)$ and θ_k, $(k = 1, 2)$ are defined as (Asadpoure and Mohammadi 2007):

$$g_k(\theta) = \sqrt{(\cos\theta + \mu_{kx}\sin\theta)^2 + (\mu_{ky}\sin\theta)^2} \quad (27)$$

$$\theta_k = \text{arctg}\left(\frac{\mu_{ky}\sin\theta}{\cos\theta + \mu_{kx}\sin\theta}\right) \quad (28)$$

where $\mu_k = \mu_{kx} + i\mu_{ky}$ are the roots of Eq. 4.

3.2 XFEM dynamic equations of motion

Consider a body Ω with an initial traction-free crack Γ_c in the state of dynamic equilibrium, as depicted in Fig. 4. The fundamental elastodynamic equation can be expressed as:

$$\nabla\cdot\boldsymbol{\sigma} + \mathbf{f}^{b} = \rho\ddot{\mathbf{u}} \quad (29)$$

with the following boundary conditions:

$$\boldsymbol{u}(\boldsymbol{x},t) = \bar{\mathbf{u}}(\mathbf{x},t) \quad \text{on } \Gamma_u \quad (30)$$

$$\boldsymbol{\sigma}\cdot\mathbf{n} = \mathbf{f}^{t} \quad \text{on } \Gamma_t \quad (31)$$

$$\boldsymbol{\sigma}\cdot\mathbf{n} = 0 \quad \text{on } \Gamma_c \quad (32)$$

and initial conditions:

$$\mathbf{u}(\mathbf{x}, t=0) = \bar{\mathbf{u}}(0) \quad (33)$$

$$\dot{\mathbf{u}}(\mathbf{x}, t=0) = \bar{\dot{\mathbf{u}}}(\mathbf{0}) \quad (34)$$

where Γ_t, Γ_u and Γ_c are traction, displacement and crack boundaries, respectively; $\boldsymbol{\sigma}$ is the stress tensor and $\mathbf{f}^{b}$ and $\mathbf{f}^{t}$ are the body force and external traction vectors, respectively.

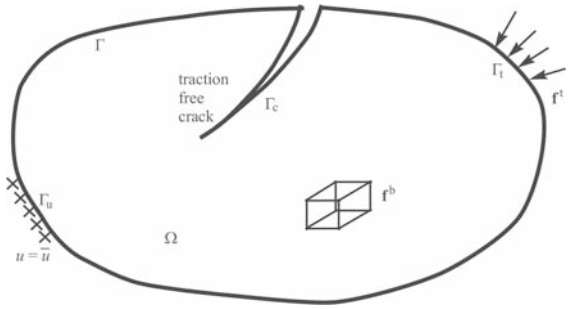

Fig. 4 A body in a state of elastodynamic equilibrium

The variational formulation of the initial/boundary value problem of Eq. 29 can be written as:

$$\int_\Omega \rho\ddot{\mathbf{u}}\cdot\delta\mathbf{u}\,d\Omega + \int_\Omega \boldsymbol{\sigma}\cdot\delta\boldsymbol{\varepsilon}\,d\Omega = \int_\Omega \mathbf{f}^{b}\cdot\delta\mathbf{u}\,d\Omega + \int_\Gamma \mathbf{f}^{t}\cdot\delta\mathbf{u}\,d\Gamma \quad (35)$$

In the extended finite element method, approximation (24) is utilized to calculate the displacement $\mathbf{u}^h(\mathbf{x})$ for a typical point $\mathbf{x}$. The discretized form of Eq. 35 using the XFEM procedure (24) can be written as:

$$\mathbf{M}\ddot{\mathbf{u}}^h + \mathbf{K}\mathbf{u}^h = \mathbf{f} \quad (36)$$

where $\mathbf{u}^h$ and $\ddot{\mathbf{u}}^h$ denote the vector of nodal parameters (displacements $\mathbf{u}$, Heaviside and crack tip enrichment degrees of freedom $\mathbf{a}$ and $\mathbf{b}$, respectively) and its second time derivative, respectively:

$$\mathbf{u}^h = \{\mathbf{u}, \mathbf{a}, \mathbf{b}\}^{T} \quad (37)$$

The stiffness matrix $\mathbf{K}$, mass matrix $\mathbf{M}$ and the external load vector $\mathbf{f}$ are defined as:

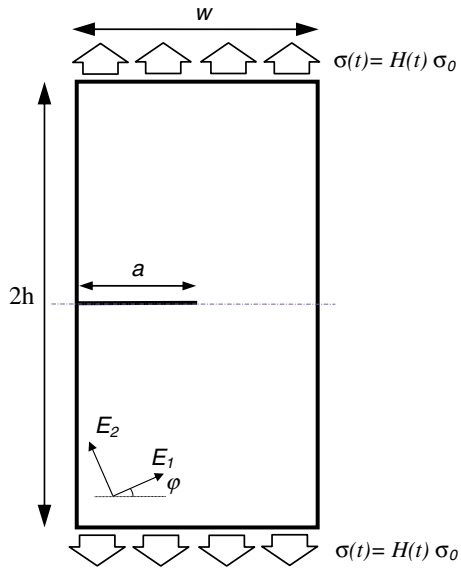

Fig. 5 Geometry and loadings of a single edge crack in a rectangular plate with several orientations of the axes of orthotropy

$$\mathbf{K}_{ij}^{e} = \begin{bmatrix} \mathbf{K}_{ij}^{\mathbf{uu}} & \mathbf{K}_{ij}^{\mathbf{ua}} & \mathbf{K}_{ij}^{\mathbf{ub}} \\ \mathbf{K}_{ij}^{\mathbf{au}} & \mathbf{K}_{ij}^{\mathbf{aa}} & \mathbf{K}_{ij}^{\mathbf{ab}} \\ \mathbf{K}_{ij}^{\mathbf{bu}} & \mathbf{K}_{ij}^{\mathbf{ba}} & \mathbf{K}_{ij}^{\mathbf{bb}} \end{bmatrix} \tag{38}$$

$$\mathbf{M}_{ij}^{e} = \begin{bmatrix} \mathbf{M}_{ij}^{\mathbf{uu}} & \mathbf{M}_{ij}^{\mathbf{ua}} & \mathbf{M}_{ij}^{\mathbf{ub}} \\ \mathbf{M}_{ij}^{\mathbf{au}} & \mathbf{M}_{ij}^{\mathbf{aa}} & \mathbf{M}_{ij}^{\mathbf{ab}} \\ \mathbf{M}_{ij}^{\mathbf{bu}} & \mathbf{M}_{ij}^{\mathbf{ba}} & \mathbf{M}_{ij}^{\mathbf{bb}} \end{bmatrix} \tag{39}$$

$$\mathbf{f}_{i} = \left\{ \mathbf{f}_{i}^{\mathbf{u}}, \mathbf{f}_{i}^{\mathbf{a}}, \mathbf{f}_{i}^{\mathbf{b}} \right\}^{\mathrm{T}} \tag{40}$$

where the stiffness components $\mathbf{K}_{ij}^{rs}(r, s = \mathbf{u}, \mathbf{a}, \mathbf{b})$ include the classical FEM (**uu**), Heaviside enrichment (**aa**), orthotropic crack tip enrichment (**bb**) and the coupled parts of XFEM approximation:

$$\mathbf{K}_{ij}^{rs} = \int_{\Omega^{\mathrm{e}}} (\mathbf{B}_{i}^{r})^{\mathrm{T}} \mathbf{D} \mathbf{B}_{j}^{s} \mathrm{d}\Omega \quad (r, s = \mathbf{u}, \mathbf{a}, \mathbf{b}) \tag{41}$$

where $\mathbf{B} = \nabla \mathbf{N}$ is the matrix of derivatives of shape functions, defined as:

$$\mathbf{B}_{i}^{\mathbf{u}} = \begin{bmatrix} N_{i,x} & 0 \\ 0 & N_{i,y} \\ N_{i,y} & N_{i,x} \end{bmatrix} \tag{42}$$

$$\mathbf{B}_{i}^{\mathbf{a}} = \begin{bmatrix} (N_i H)_{,x} & 0 \\ 0 & (N_i H)_{,y} \\ (N_i H)_{,y} & (N_i H)_{,x} \end{bmatrix} \tag{43}$$

$$\mathbf{B}_{i}^{\mathbf{b}} = \begin{bmatrix} \mathbf{B}_{i}^{\mathbf{b}_1} & \mathbf{B}_{i}^{\mathbf{b}_2} & \mathbf{B}_{i}^{\mathbf{b}_3} & \mathbf{B}_{i}^{\mathbf{b}_4} \end{bmatrix} \tag{44}$$

$$\mathbf{B}_{i}^{\mathbf{b}_\alpha} = \begin{bmatrix} (N_i \mathrm{F}_\alpha)_{,x} & 0 \\ 0 & (N_i \mathrm{F}_\alpha)_{,y} \\ (N_i \mathrm{F}_\alpha)_{,y} & (N_i \mathrm{F}_\alpha)_{,x} \end{bmatrix} \quad (\alpha = 1, 2, 3 \text{ and } 4) \tag{45}$$

To include the effects of interpolation, the following shifting amendments are required (Mohammadi 2008):

$$\mathbf{B}_{i}^{\mathbf{a}} = \begin{bmatrix} (N_i [H(\xi) - H(\xi)])_{,x} & 0 \\ 0 & (N_i [H(\xi) - H(\xi_i)])_{,y} \\ (N_i [H(\xi) - H(\xi)])_{,y} & (N_i [H(\xi) - H(\xi_i)])_{,x} \end{bmatrix} \tag{46}$$

$$\mathbf{B}_{i}^{\mathbf{b}_\alpha} = \begin{bmatrix} [N_i (\mathrm{F}_\alpha - \mathrm{F}_{\alpha i})]_{,x} & 0 \\ 0 & [N_i (\mathrm{F}_\alpha - \mathrm{F}_{\alpha i})]_{,y} \\ [N_i (\mathrm{F}_\alpha - \mathrm{F}_{\alpha i})]_{,y} & [N_i (\mathrm{F}_\alpha - \mathrm{F}_{\alpha i})]_{,x} \end{bmatrix} (\alpha = 1, 2, 3 \text{ and } 4) \tag{47}$$

Classical and enrichment components of the consistent mass matrix can be expressed as:

$$\mathbf{M}_{ij}^{\mathbf{uu}} = \int_{\Omega} \rho N_i N_j \, \mathrm{d}\Omega \tag{48}$$

$$\mathbf{M}_{ij}^{\mathbf{aa}} = \int_{\Omega} \rho (N_i H_i)(N_j H_j) \mathrm{d}\Omega \tag{49}$$

$$\mathbf{M}_{ij}^{\mathbf{bb}} = \int_{\Omega} \rho \, (N_i \mathrm{F}_{\alpha i}) \left(N_j \mathrm{F}_{\alpha j} \right) \mathrm{d}\Omega \quad (\alpha = 1, 2, 3 \text{ and } 4) \tag{50}$$

$$\mathbf{M}_{ij}^{\mathbf{ua}} = \mathbf{M}_{ij}^{\mathbf{au}} = \int_{\Omega} \rho N_i^{(N_j H_j)} \mathrm{d}\Omega \tag{51}$$

$$\mathbf{M}_{ij}^{\mathbf{ub}} = \mathbf{M}_{ij}^{\mathbf{bu}} = \int_{\Omega} \rho N_i \left(N_j \mathrm{F}_{\alpha j} \right) \mathrm{d}\Omega \times (\alpha = 1, 2, 3 \text{ and } 4) \tag{52}$$

$$\mathbf{M}_{ij}^{\mathbf{ab}} = \int_{\Omega} \rho (N_i H_i)(N_j \mathrm{F}_{\alpha j}) \mathrm{d}\Omega \quad (\alpha = 1, 2, 3 \text{ and } 4) \tag{53}$$

Finally, the force vectors associated with the classical and enrichment degrees of freedom are defined as:

$$\mathbf{f}_{i}^{\mathbf{u}} = \int_{\Gamma_{\mathrm{t}}} N_i \mathbf{f}^{\mathrm{t}} \, \mathrm{d}\Gamma + \int_{\Omega^e} N_i \mathbf{f}^{\mathrm{b}} \, \mathrm{d}\Omega \tag{54}$$

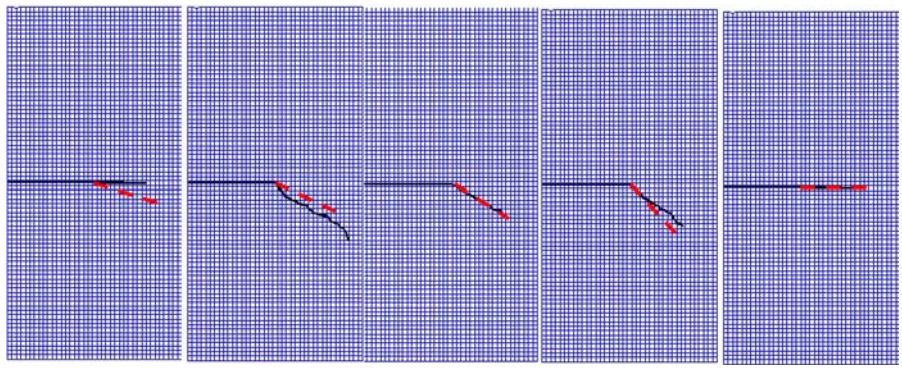

Fig. 6 Crack paths for a single edge crack plate for $\varphi = 0°, 30°, 45°, 60°$ and $90°$ material angles; the present work (straight-line) and Aliabadia and Sollero (1998) (dash-line)

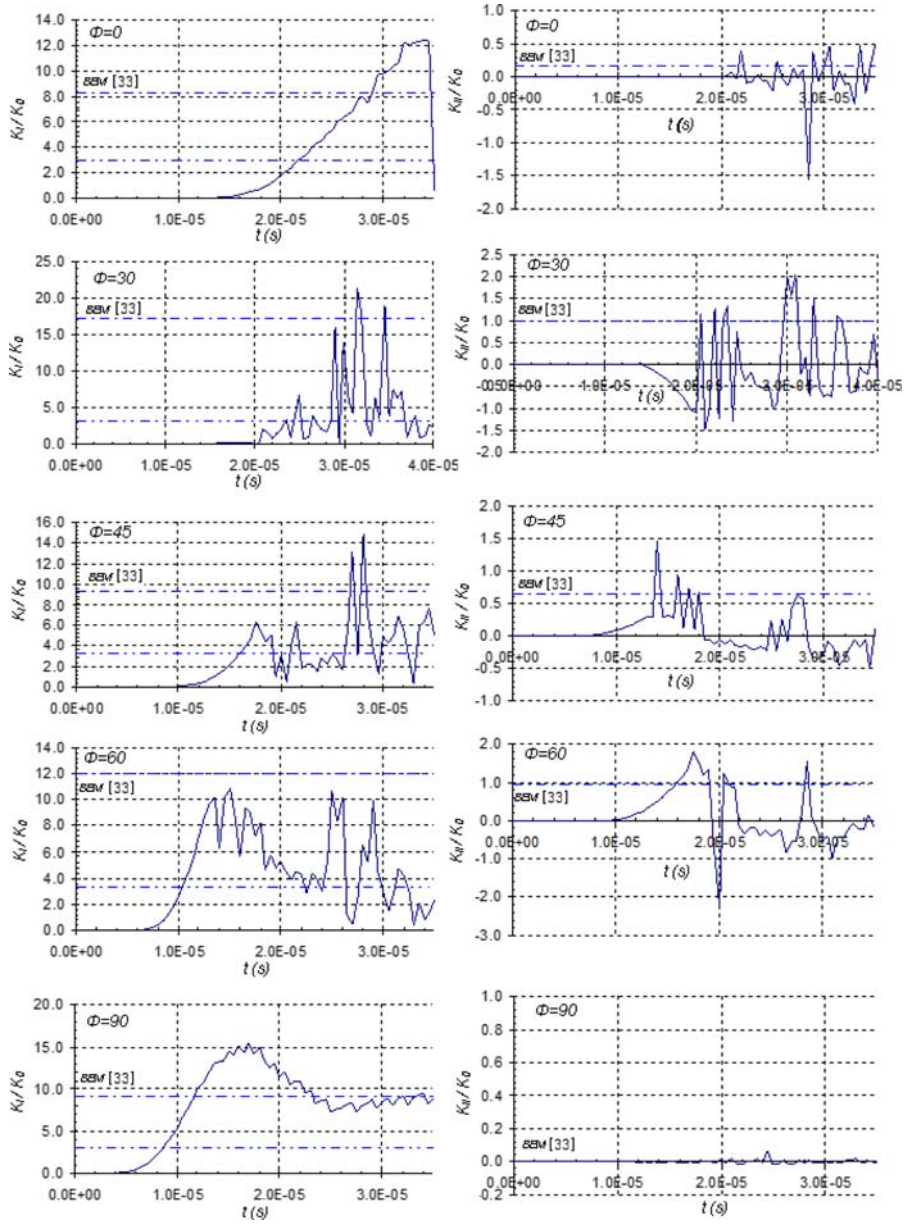

Fig. 7 Dynamic stress intensity factors for a single edge crack plate with $\varphi = 0°, 30°, 45°, 60°$ and $90°$ material angles

$$\mathbf{f}_i^{\mathbf{a}} = \int_{\Gamma_t} N_i H \mathbf{f}^{\mathrm{t}} \, \mathrm{d}\Gamma + \int_{\Omega^e} N_i H \mathbf{f}^{\mathrm{b}} \, \mathrm{d}\Omega \tag{55}$$

$$\mathbf{f}_i^{\mathbf{b}} = \int_{\Gamma_t} N_i \mathrm{F}_\alpha \mathbf{f}^{\mathrm{t}} \, \mathrm{d}\Gamma + \int_{\Omega^e} N_i \mathrm{F}_\alpha \mathbf{f}^{\mathrm{b}} \, \mathrm{d}\Omega \quad (\alpha = 1, 2, 3 \text{ and } 4) \tag{56}$$

It is also possible to similarly extend the formulation to include the effects of velocity based global damping,

$$\mathbf{M}\ddot{\mathbf{u}}^h + \mathbf{C}\dot{\mathbf{u}}^h + \mathbf{K}\mathbf{u}^h = \mathbf{f} \tag{57}$$

The Newmark time integration scheme is then adopted to solve for the extended finite element equation of motion at time step n:

$$\mathbf{M}\ddot{\mathbf{u}}_n^h + \mathbf{C}\dot{\mathbf{u}}_n^h + \mathbf{K}\mathbf{u}_n^h = \mathbf{f}_n \tag{58}$$

where $\mathbf{M}_n$, $\mathbf{K}_n$ and $\mathbf{C}_n$ are the mass, stiffness and damping matrices, respectively, and $\mathbf{f}_n$ is the load vector at the time step n. The final discretized simultaneous equations are expressed as:

$$\left(M+\beta\Delta t^2K+\alpha\Delta tC\right)\ddot{u}_n^h = f_n - K\left(u_{n-1}^h+\Delta t\dot{u}_{n-1}^h+(1-2\beta)\frac{\Delta t^2}{2}\ddot{u}_{n-1}^h\right) -C\left(\dot{u}_{n-1}^h+(1-\alpha)\Delta t\ddot{u}_{n-1}^h\right) \quad (59)$$

$$\dot{u}_n^h = \dot{u}_{n-1}^h+(1-\alpha)\Delta t\ddot{u}_{n-1}^h+\alpha\Delta t\ddot{u}_n^h \quad (60)$$

$$u_n^h = u_{n-1}^h+\Delta t\dot{u}_{n-1}^h +(1-2\beta)\frac{\Delta t^2}{2}\ddot{u}_{n-1}^h+\beta\Delta t^2\ddot{u}_n^h \quad (61)$$

The choice of $\alpha = 1/2$ and $\beta = 1/4$, unconditionally guarantees the stability of the Newmark approach.

In the following simulations, a similar technique proposed by Combescure et al. (2008) and Réthoré et al. (2005) has been used. In this method, no degree of freedom is eliminated after crack propagation. In this way, only more degrees of freedom are added relative to the crack-tip enriched elements and previous crack-tip enriched elements are changed to Heaviside enriched elements. The degrees of freedom associated with crack-tip enrichments from a previous step are still stored and used in calculations, but their singularity effect will be diminished by the increasing distance between the nodes associated with previous crack-tip and the new crack-tip position. The same references have illustrated that the energy conservation is well preserved. So, the acceleration which is calculated by the Newmark scheme, will remain reliable for post-processing purposes

4 Numerical examples

In this section, the performance of the proposed method is investigated by simulation of a number of problems. The robustness and accuracy of the method are compared with other available theoretical or numerical approaches. Three examples are studied which include an edge crack tensile plate in quasi-static state, an orthotropic plate subjected to impulse loading, and finally a pre-cracked beam under dynamic loading. A comprehensive parametric study is provided to assess the sensitivity of the results with respect to the primary parameters of XFEM.

4.1 Edge crack in a composite plate under tensile stress loading

This example was studied by Aliabadia and Sollero (1998) in a quasi-static condition. Let's consider a rectangular plate with an edge horizontal crack subjected to a tensile distributed loading (Fig. 5). 0, 30, 45, 60 and 90 material orientation angles are studied and the plane stress state is presumed. The size of the cracked plate is h = w = 50 mm and a = 25 mm. Graphite-epoxy material properties are assumed to be the following orthotropic properties, $E_1 = 114.8$ GPa , $E_2 = 11.7$ GPa , $G_{12} = 9.66$ GPa , $\upsilon_{12} = 0.21$ and $\rho = 1500\,\mathrm{kg/m^3}$. The time-step is selected to be $\Delta t = 0.5\,\mu$s and the relative integration domain size, r_d/a, is set to be 0.4. A 40×80 mesh is used for the finite element mesh. The integrations are performed by

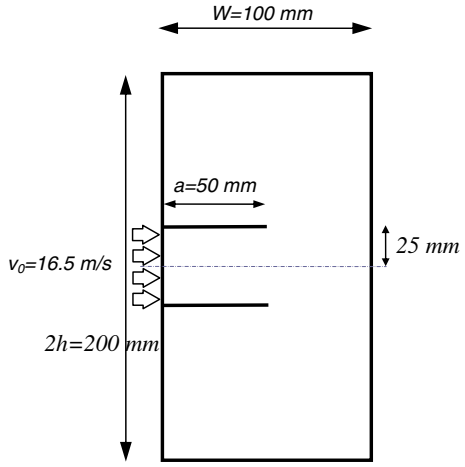

Fig. 8 Geometry and boundary condition of the double edge crack in a rectangular plate

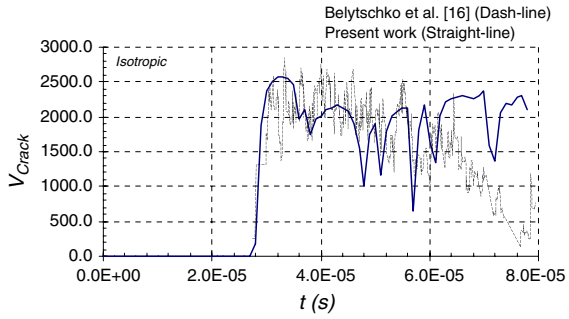

Fig. 9 The crack propagation speed for Kalthoff's (1987) experiment, the loss of hyperbolicity criterion (Dash-line) and the maximum hoop stress (Straight-line)

4×4 and 7×7 Gauss quadrature rules for ordinary and enriched elements, respectively. The same integration rule is applied to all other examples.

Figure 6 illustrates the predicted crack propagation paths for different orthotropic material angles, and compares them with the reference results (Aliabadia and Sollero 1998). Good agreement is observed except for the first case, where the orthotropic material axes are parallel/perpendicular to the initial crack face. The present approach predicts an extension along the crack direction, whereas Aliabadia and Sollero (1998) predicted an inclined propagation. The reason might be attributed to the fact that the reference approach might have included bifurcation and instability analysis which have resulted

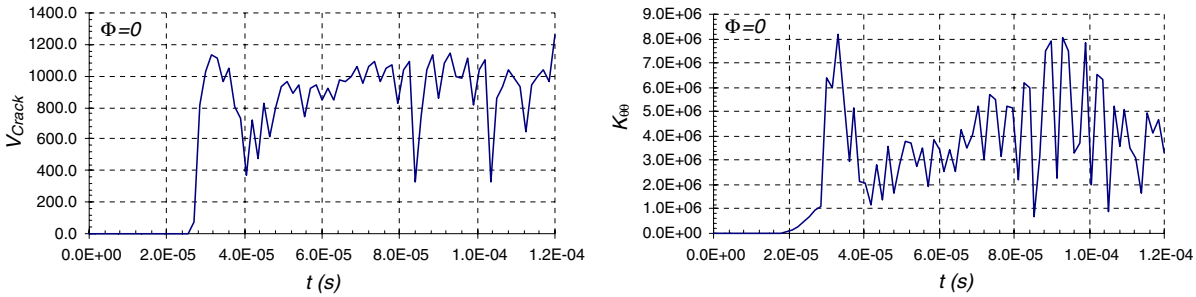

Fig. 10 The crack propagation speed and the maximum hoop stress intensity factor for Kalthoff's (1987) experiment with the maximum hoop criterion

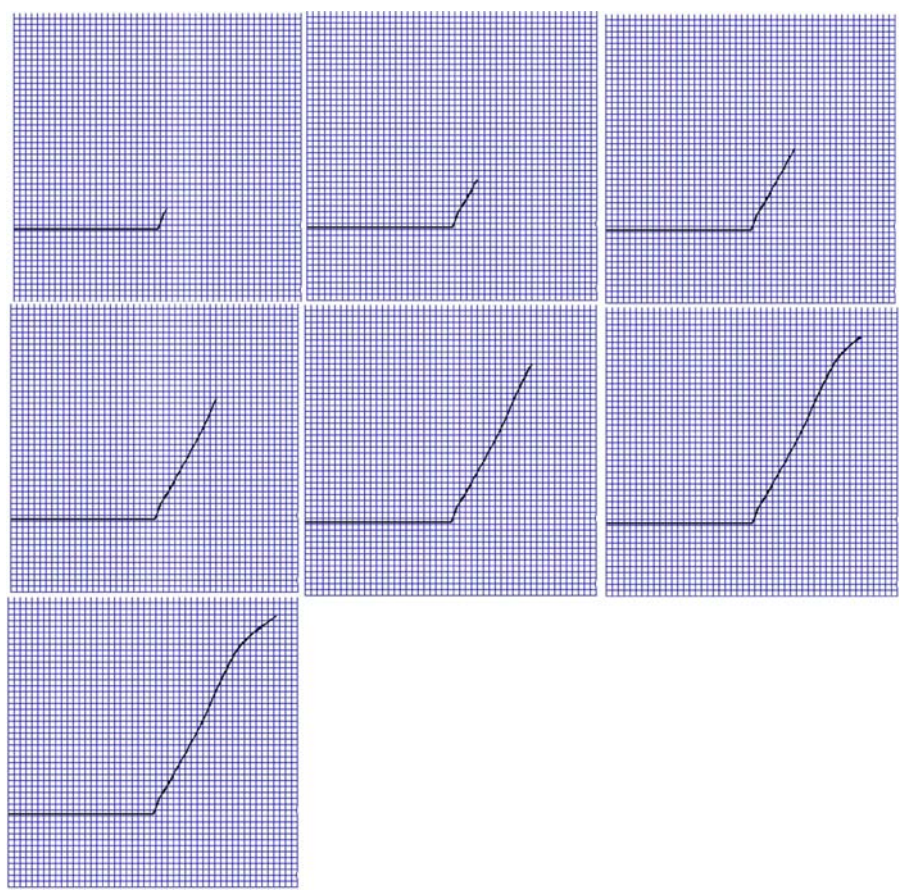

Fig. 11 The crack growth path for Kalthoff's (1987) experiment with the maximum hoop criterion at times $t = 25, 35, 45, 55, 65, 75$ and $80\,\mu$s

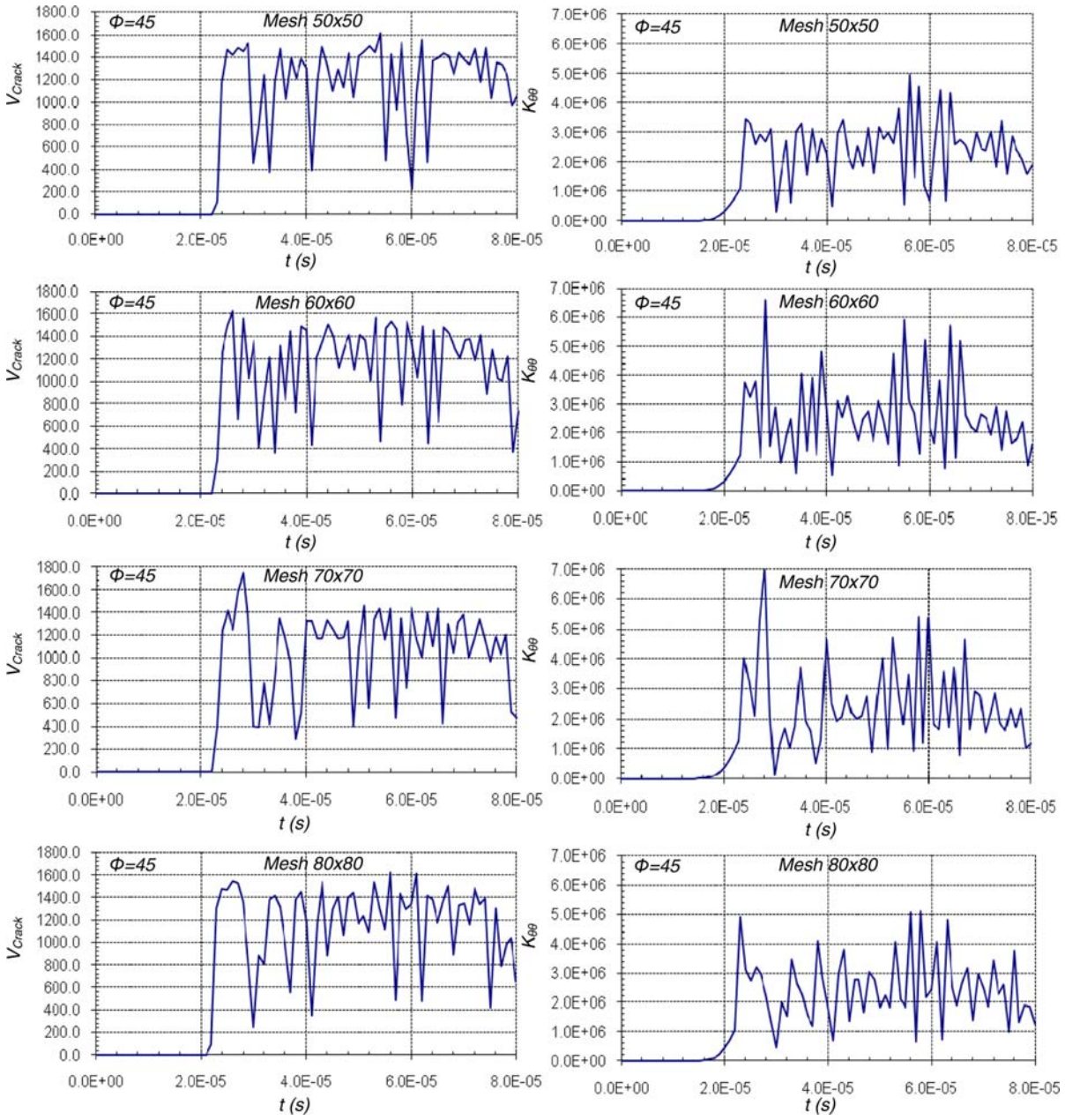

Fig. 12 The crack propagation speed and the maximum hoop stress intensity factor with orientation angle of 45° and different meshes

in an un-symmetric inclined extension, which clearly required lower level of energy compared with a straight symmetric crack extension. The present approach, however, does not include such an instability analysis and a symmetric response is expected from a fully symmetric problem.

The predicted time histories of mode I and mode II dynamic stress intensity factors are illustrated in Fig. 7. The results for different orthotropic material angles $\varphi = 0°, 30°, 45°, 60°$ and 90° have been compared with the maximum and minimum quasi-static solutions of Aliabadia and Sollero (1998), obtained from a boundary element formulation (The reference minimum solution for K_{II} was zero; x-axis). The results show that the maximum values of mode I dynamic stress intensity factor vary similar to the reference

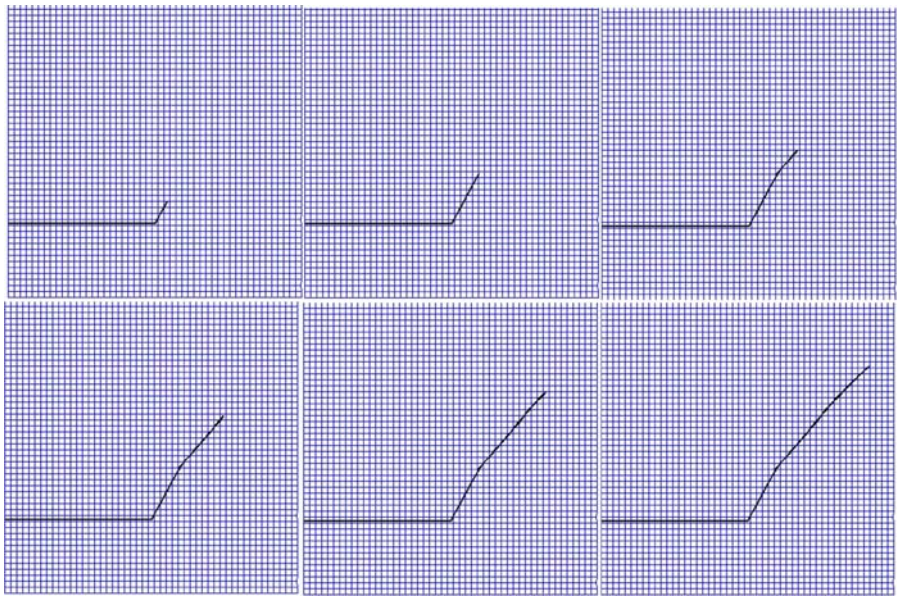

Fig. 13 The crack growth path with orientation angle of 45° and 50 × 50 mesh at times $t = 30, 40, 50, 60, 70$ and 80 μs

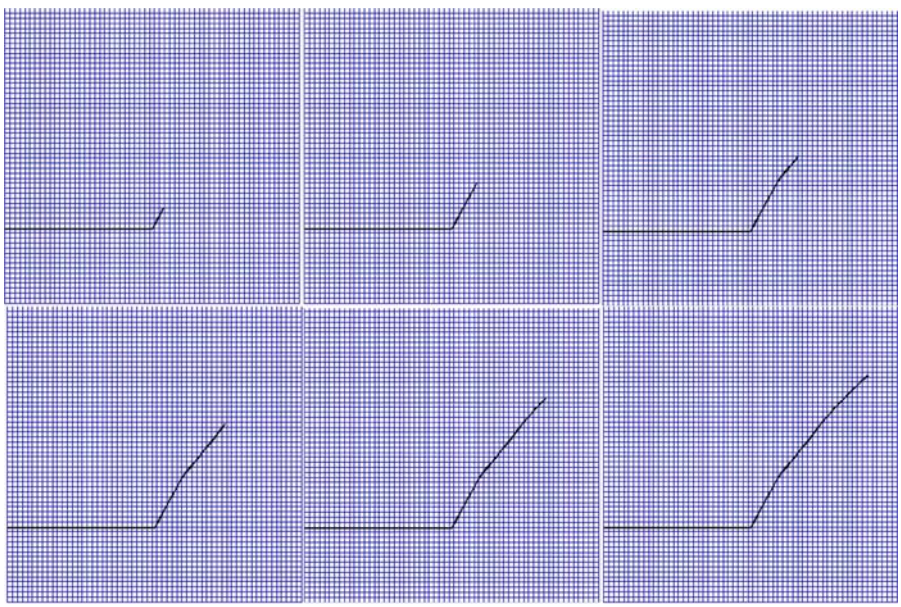

Fig. 14 The crack growth path with orientation angle of 45° and 60 × 60 mesh at times $t = 30, 40, 50, 60, 70$ and 80 μs

results by increasing φ. The maximum value of mode I dynamic stress intensity factor occurs for the case of $\varphi = 30°$, which is similar to the conclusion of Aliabadia and Sollero (1998). Generally, an acceptable trend is observed, while the present dynamic solutions oscillate about an average solution; i.e. more or less similar to the quasi-static response.

4.2 A composite plate with double edge cracks under impulsive loading

This problem was investigated experimentally by Kalthoff and Winkler (1987) and then numerically studied by Belytschko and Chen (2004). In this problem, a plate with two edge notches is impacted by a

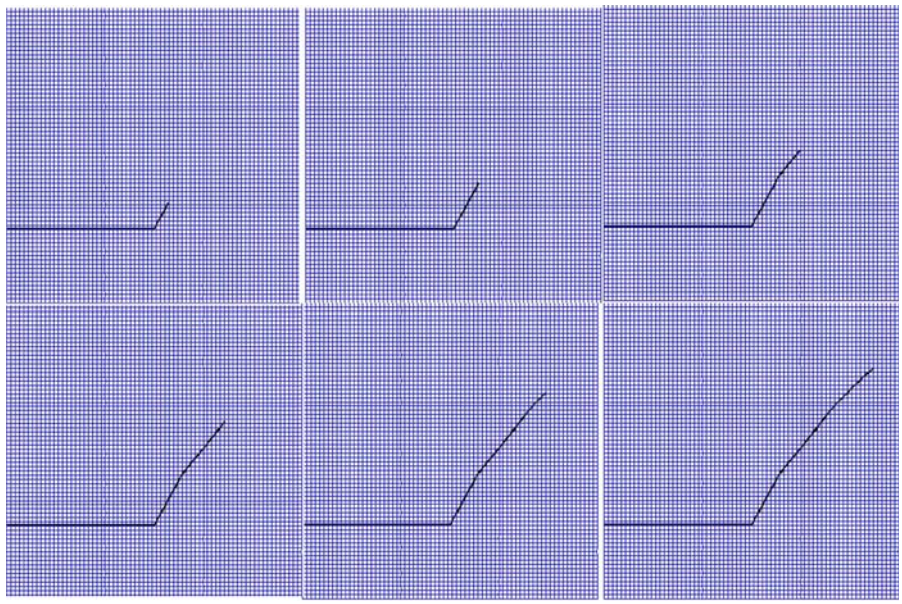

Fig. 15 The crack growth path with orientation angle of 45° and 70 × 70 mesh at times $t = 30, 40, 50, 60, 70$ and 80 μs

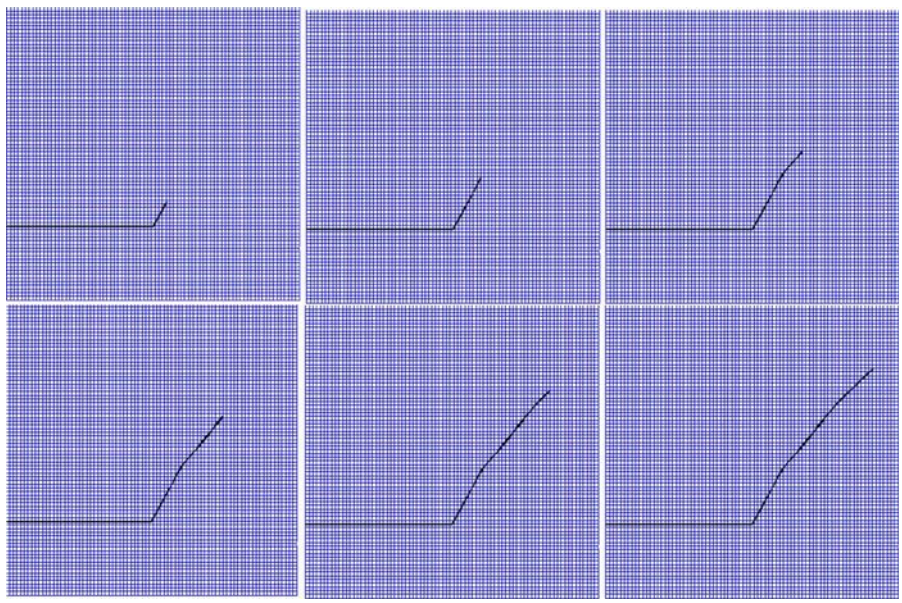

Fig. 16 The crack growth path with orientation angle of 45° and 80 × 80 mesh at times $t = 30, 40, 50, 60, 70$ and 80 μs

projectile, as depicted in Fig. 8. Kalthoff and Winkler (1987) showed that a lower projectile speed will cause a lower strain rate and a brittle fracture mode. In lower strain rates, a crack propagation angle of approximately 70° was observed.

In this example, the material is first simulated as an isotropic material in order to compare the results of the present approach with the isotropic approach by Belytschko and Chen (2004), which was based on the loss of hyperbolicity criterion. Then, the same problem is solved for orthotropic composites and the effects of different finite element meshes are investigated.

In Belytschko and Chen (2004), the impulse was considered as a boundary speed condition. For low strain rates, this speed was assumed equal to 16.5 m/s, according to Kalthoff and Winkler (1987).

The material properties correspond to maraging steel type 18Ni1900: $E = 190$ GPa , $\upsilon = 0.3$ and

$\rho = 8000\ \mathrm{kg/m^3}$. The critical stress intensity factor is considered to be $K_{Ic} = 68\ \mathrm{MPa}\sqrt{m}$. The dilatational, shear and Rayleigh wave speeds are $C_d = 5654.3$ m/s, $C_s = 3022.4$ m/s and $C_R = 2799.2$ m/s, respectively.

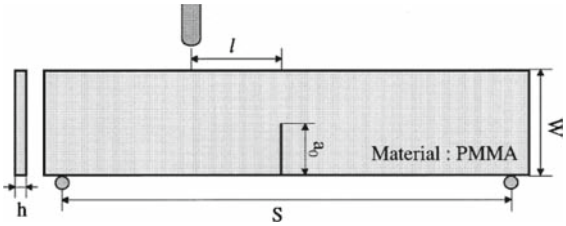

Fig. 17 A three point bending specimen under impact loading (Nishioka et al. 2001)

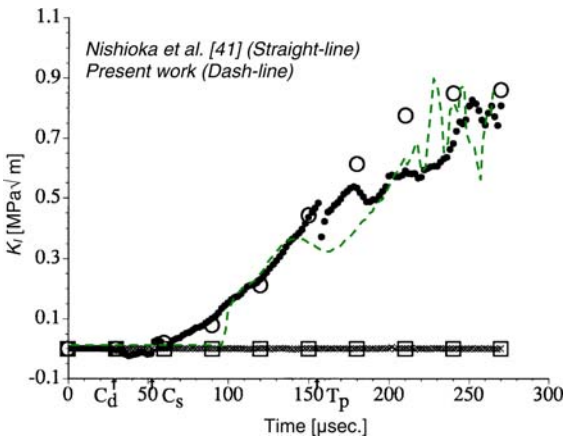

Fig. 18 Comparison of the mode I dynamic stress intensity factor for $e = 0.0$

The simulation is performed up to 80 μs and the timestep is considered $\Delta t = 1\ \mu$s. The relative integration domain size, r_d/a, is selected to be 0.4 and only one half of the plate is modeled, due to symmetry, by a 50×50 finite element mesh.

Figure 9 depicts the time history of the crack propagation speed and compares it with the reference isotropic results. According to the results, the crack starts to propagate at $t = 27\ \mu$s, matching the initiation time $t = 26.17\ \mu$s reported by Belytschko and Chen (2004). Variations of the crack tip speed is comparable with Belytschko and Chen (2004) results, except for the last part of crack evolution, which starts at $t = 50\ \mu$s. This difference may have caused from the fact that the methods have used different definitions for estimation of the crack speed.

The predicted crack initiation angle is 67.5° and during the crack growth, the angle varies and gradually decreases to 59.4°, which is matched with both Kalthoff and Winkler (1987) and Belytschko and Chen (2004) references.

Now, the same problem is considered as an orthotropic material with the following properties: $E_1 = 8.6$ GPa, $E_2 = 39$ GPa , $E_3 = 12$ GPa , $G_{12} = 3.8$ GPa , $v_{12} = 0.061$, $v_{23} = 0.04$, $v_{13} = 0.23$ and $\rho = 2100\ \mathrm{kg/m^3}$. The critical stress intensity factor is considered to be $K_{Ic} = 1\mathrm{MPa}\sqrt{m}$ and the dilatational, shear and Rayleigh wave speeds $\Phi = 45$ are $C_d = 2071.3$ m/s, $C_s = 1545.2$ m/s, and $C_R = 1345.6$ m/s, respectively. The time-step is selected to be $\Delta t = 1.5\ \mu$s and the relative integration domain size, r_d/a, is set to be 0.4. A 50×50 finite element mesh is implemented to model half of the plate. Also, the impact speed is

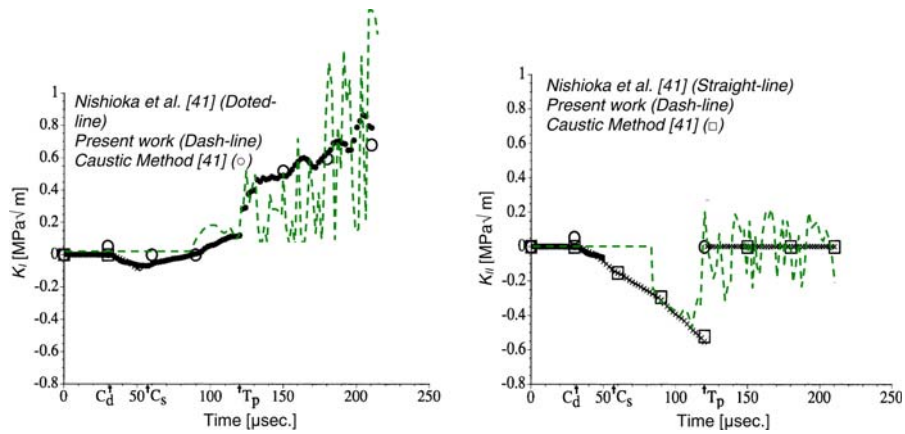

Fig. 19 Comparison of mixed-mode dynamic stress intensity factors for $e = 0.1$

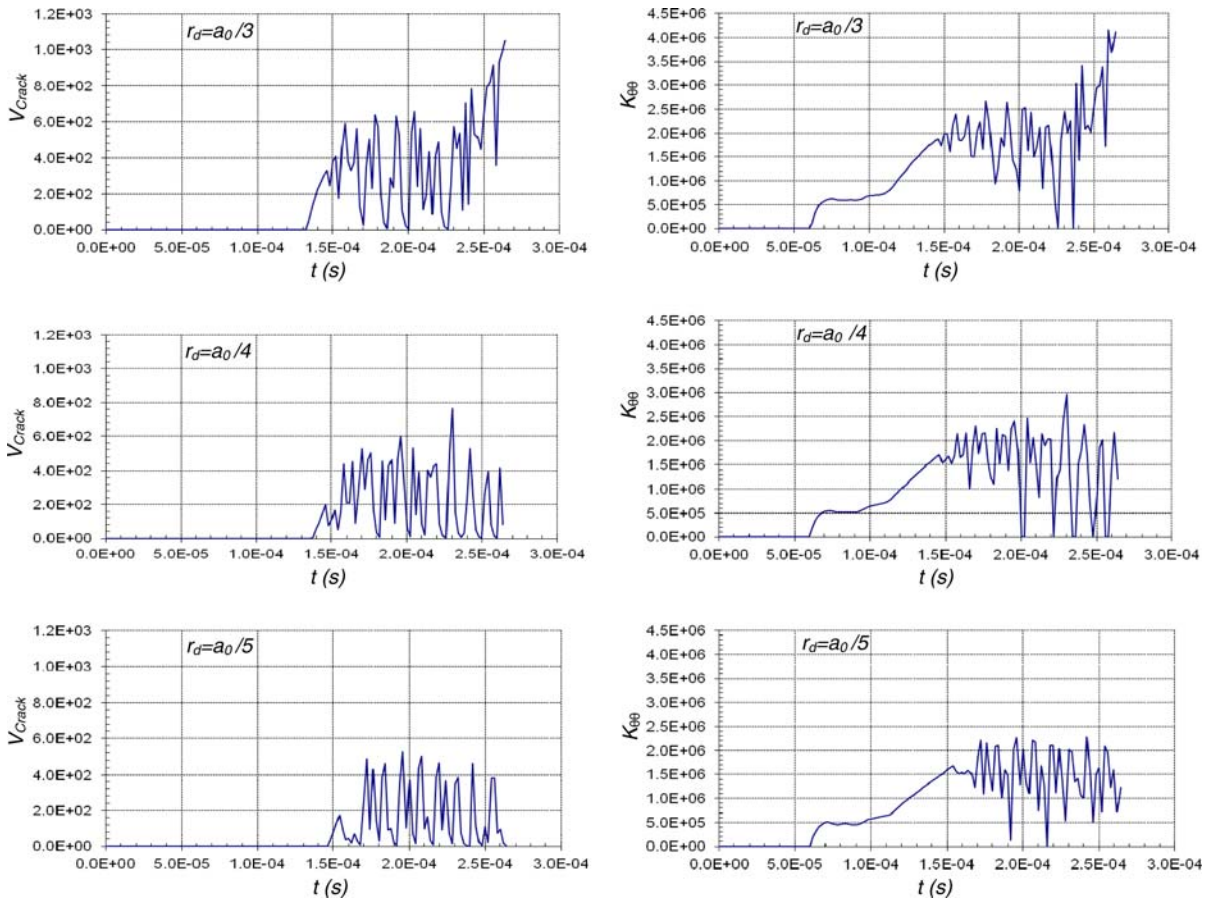

Fig. 20 Effect of different relative integration domain sizes, r_d/a, for $e = 0.0$

reduced to 5 m/s in order to ensure the low strain rate condition.

According to the results, depicted in Fig. 10, the crack starts to propagate at $t = 25\,\mu$s. The crack tip speed changes from 72.4 to 1142.3 m/s. Propagation patterns are shown in Fig. 11, which shows that the initial notch propagates with an initiation angle of 63.4° at time 25 μs and then decreases to 54.1° at the end of crack growth at 80 μs.

In order to evaluate the effects of different finite element meshes on dynamic crack propagation, four different meshes 50×50, 60×60, 70×70 and 80×80 are utilized. The material angle is considered to be 45° and the time-step is chosen to be $\Delta t = 1\,\mu$s. The results, depicted in Fig. 12, show good agreement for crack growth path and crack tip speed in all simulations, notably even when the speed is reached to 1627 m/s at the maximum point. In average, the crack angle at initiation remains at about 63.4° and then decreases to about 50.1° at the end of analysis. Such a decreasing trend in crack angle propagation has probably been caused by the effects of reflected waves from the right side boundary of plate.

Figures 13,14,15, and 16 illustrate the crack propagation paths at six successive times $t = 30$, 40, 50, 60, 70 and 80 μs for four different finite element meshes; 50×50, 60×60, 70×70 and 80×80. Similar results are observed which indicate the mesh independency of the results.

4.3 Pre-cracked beam under impact loading

For the final example, a pre-cracked beam previously investigated by Nishioka et al. (2001) with isotropic properties, is investigated. In this problem, a three point bending beam is studied under a projectile impulse

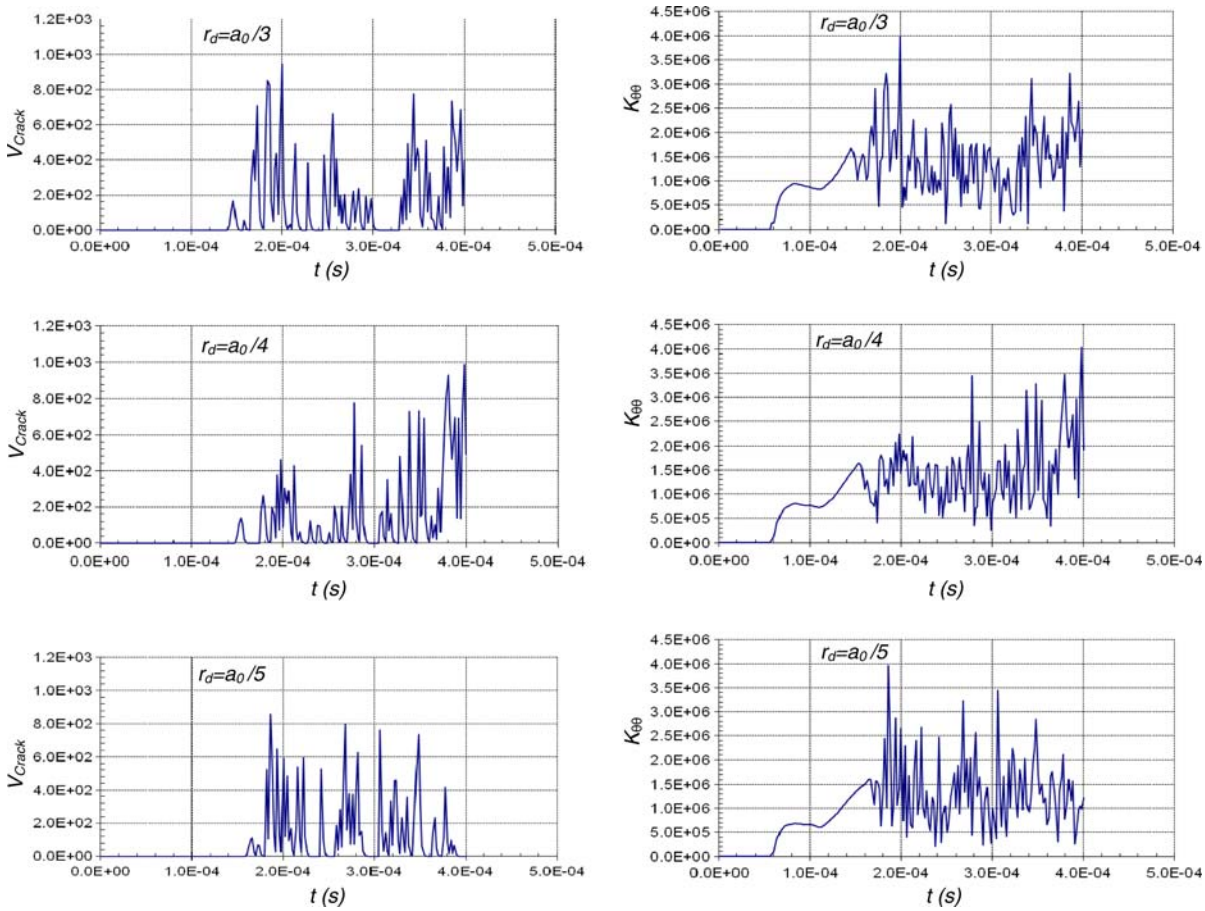

Fig. 21 Effect of different relative integration domain sizes, r_d/a, for $e = 0.1$

with 5 m/s, as depicted in Fig. 17. The dimensions are: $L = 0.43$ m, $W = 0.1$ m, $S = 0.4$ m, $h = 0.01$ m, $a_0 = 0.05$ m. The material properties are $E = 2.94$ GPa, $v = 0.3$ and $\rho = 1190$ kg/m^3. The critical stress intensity factor is considered to be $K_{Ic} = 4.6$ MPa$\sqrt{m}$. The dilatational wave speed is $C_d = 1710$ m/s, whereas the shear wave speed is $C_s = 941$ m/s. In order to investigate various effects of mixed mode fracture, different eccentricities of loading, defined as $e = 2l/S$, are considered. The time-step is considered as $\Delta t = 2\,\mu$s and a 120×40 finite element mesh is chosen to discretize the model.

Figure 18 compares the results of the proposed approach with the reference results by Nishioka et al. (2001) for the zero eccentricity $e = 0.0$. The results match well in this case, whereas when the eccentricity increases, although the results show the same trend, but slightly different results are obtained (Fig. 19). The reason may be attributed to the different adopted propagation criterion in Nishioka et al. (2001), where an iterative procedure was used to find the minimum K_2. This difference is minimized (vanished) for the symmetric condition of zero eccentricity, as the same results are obtained from the both propagation criteria.

Furthermore, the simulation is extended to an orthotropic material with the following properties: $E_1 = 8.6$ GPa, $E_2 = 39$ GPa, $E_3 = 12$ GPa, $G_{12} = 3.8$ GPa, $v_{12} = 0.061$, $v_{23} = 0.04$, $v_{13} = 0.23$ and $\rho = 2100$kg/m^3. The critical stress intensity factor is considered to be $K_{Ic} = 1$ MPa$\sqrt{m}$ and the dilatational, shear and Rayleigh wave speeds are $C_d = 2071.3$ m/s, $C_s = 1545.2$ m/s, and $C_R = 1345.6$ m/s, respectively. Different results for crack propagation velocity and the stress intensity factor, obtained from different relative integration domain sizes, r_d/a, are compared in Fig. 20. The dynamic stress intensity factors are seemingly the

same. Existing differences may have caused because of the effect of the impact wave on the domain elements in different times. In the case of $e = 0.0$, the crack starts to initiate at $t = 140\,\mu s$ (Fig. 20), while for $e = 0.1$ this time is $t = 125\,\mu s$ (Fig. 21). After each evolution during the crack propagation, the energy release rate reduces to a value lower than the critical level. As a result, the crack tip will rest until the energy reaches the critical value during the upcoming time steps.

The speed of crack tip varies based on the integration domain size and eccentricity, but their trends and crack propagation paths remain similar.

5 Conclusion

In this study, a new method has been presented for modeling crack evolution in orthotropic materials. Orthotropic crack tip enrichment functions are implemented in the extended finite element method (XFEM) to simulate the dynamic crack propagation in composites. A simple crack propagation criterion based on dynamic stress intensity factors and energy release rate is adopted. The results have been compared with available benchmarks and demonstrated close agreement. The predicted crack propagation patterns were similar and the crack tip velocities were in good agreement with previous numerical and experimental results. Also, the robustness of the method unveiled by using different sizes of mesh and different domain sizes for J-integral evaluation which disclosed independency of the proposed method from changing the mesh size and domain size. Moreover, it was demonstrated that the static crack tip enrichment functions were able to correctly simulate the crack tip displacement and stress field, as well as the propagation paths.

References

Aliabadia MH, Sollero P (1998) Crack growth analysis in homogeneous orthotropic laminates. Compos Sci Technol 58:1697–1703

Areias PMA, Belytschko T (2005) Analysis of three-dimensional crack initiation and propagation using the extended finite element method. Int J Numer Meth Eng 63:760–788

Asadpoure A, Mohammadi S (2007) Developing new enrichment functions for crack simulation in orthotropic media by the extended finite element method. Int J Numer Methods Eng 69:25150–25172

Asadpoure A, Mohammadi S, Vafai A (2006a) Crack analysis in orthotropic media using the extended finite element method. Thin-Walled Struct 44(9):1031–1038

Asadpoure A, Mohammadi S, Vafai A (2006b) Modeling crack in orthotropic media using a coupled finite element and partion of unity methods. Finite Elem Anal Des 42(13): 1165–1175

Atluri SN, Kobayashi AS, Nakagaki M (1975) A finite element program for fracture analysis of composite material. In: Fracture mechanics of composites. ASTM STP 593. American Society for Testing and Materials, Philadelphia, PA

Belytschko T, Black T (1999) Elastic crack growth in finite elements with minimal remeshing. Int J Numer Meth Eng 45:601–620

Belytschko T, Chen H (2004) Singular enrichment finite element method for elastodynamic crack propagation. Int J Numer Meth Eng 1(1):1–15

Belytschko T, Chen H, Xu J, Zi G (2003) Dynamic crack propagation based on loss of hyperbolicity and a new discontinuous enrichment. Int J Numer Meth Eng 58:1873–1905

Boone TJ, Wawrzynek PA, Ingraffea AR (1987) Finite element modeling of fracture propagation in orthotropic materials. Eng Fract Mech 26:185–201

Camacho GT, Ortiz M (1996) Computational modeling of impact damage in brittle materials. Int J Solids Struct 33:2899–2938

Chessa J, Belytschko T (2004) Arbitrary discontinuities in space–time finite elements by level sets and X-FEM. Int J Numer Methods Eng 61:2595–2614

Chessa J, Belytschko T (2006) A local space–time discontinuous finite element method. Comput Methods Appl Mech Eng 195:1325–1343

Combescure A, Gravouil A, Gregoire D, Rethore J (2008) X-FEM a good candidate for energy conservation in simulation of brittle dynamic crack propagation. Comput Methods Appl Mech Eng 197:309–318

Dolbow J, Moës N, Belytschko T (2001) An extended finite element method for modeling crack growth with frictional contact. Comput Meth Appl Mech Eng 190:6825–6846

Dongye C, Ting TCT (1989) Explicit expressions of Barnett-Lothe tensors and their associated tensors for orthotropic materials. Q Appl Math 47:723–734

Forschi RO, Barret JD (1976) Stress intensity factors in anisotropic plates using singular isoparametric elements. Int J Numer Methods Eng 10:1281–1287

Gao H, Klein P (1998) Numerical simulation of crack growth in an isotropic solid with randomized internal cohesive bonds. J Mech Phys Solids 42(6):187–218

Gregoire D, Maigre H, Rethore J, Combescure A (2007) Dynamic crack propagation under mixed-mode loading—comparison between experiments and X-FEM simulations. Int J Solids Struct 44:6517–6534

Kalthoff JF, Winkler S (1987) Failure mode transition at high rates of shear loading. In: International conference on impact loading and dynamic behavior of materials, vol 1, pp 185–195

Kanninen M, Popelar CH (1985) Advanced fracture mechanics. Oxford University Press, Oxford

Kim JH, Paulino GH (2003) The interaction integral for fracture of orthotropic functionally graded materials: evalu-

ation of stress intensity factors. Int J Solids Struct 40: 3967–4001

Lekhnitskii SG (1963) Theory of an anisotropic elastic body. Holden-Day, San Francisco

Maigre H, Rittel D (1993) Mixed-mode quantification for dynamic fracture initiation: application to the compact compression specimen. Int J Solids Struct 30(23):3233–3244

Melenk JM, Babuška I (1996) The partition of unity finite element method: basic theory and applications. Comput Meth Appl Mech Eng 139:289–314

Menouillard T, Réthoré J, Combescure A, Bung H (2006) Efficient explicit time stepping for the extended finite element method (X-FEM). Int J Numer Methods Eng 68(9): 911–939

Mergheim J, Kuhl E, Steinmann P (2005) A finite element method for the computational modeling of cohesive cracks. Int J Numer Meth Eng 63:276–289

Moës N, Dolbow J, Belytschko T (1999) A finite element method for crack growth without remeshing. Int J Numer Meth Eng 46:131–150

Mohammadi S (2008) Extended finite element method. Wiley/ Blackwell

Nishioka T, Alturi SN (1984) On the computation of mixed-mode k-factors for a dynamically propagating crack, using path-independent integrals. J Eng Fract Mech 20:193–208

Nishioka T, Tokudome H, Kinoshita M (2001) Dynamic fracture-path prediction in impact fracture phenomena using moving finite element method based on Delaunay automatic mesh generation. Int J Solids Struct 38:5273–5301

Nistor I, Pantale O, Caperaa S (2008) Numerical implementation of the eXtended Finite Element Method for dynamic crack analysis. Int J Adv Eng Softw 39:573–587

Oliver J, Huespe AE, Pulido MDG, Samaniego E (2003) On the strong discontinuity approach in finite deformation settings. Int J Numer Methods Eng 56:1051–1082

Peerlings RHJ, de Borst R, Brekelmans WAM, Geers MGD (2002) Localisation issues in local and nonlocal continuum approaches to fracture. Eur J Mech A: Solids 21:175–189

Réthoré J, Gravouil A, Combescure A (2005b) A combined space–time extended finite element method. Int J Numer Methods Eng 64:260–284

Sukumar N, Moës N, Moran B, Belytschko T (2000) Extended finite element method for three-dimensional crack modeling. Int J Numer Meth Eng 48:1549–1570

Ventura G, Budyn E, Belytschko T (2003) Vector level sets for description of propagating cracks in finite elements. Int J Numer Methods Eng 58:1571–1592

Wu KC (2000) Dynamic crack growth in anisotropic material. Int J Fract 106:1–12

Xu XP, Needleman A (1994) Numerical simulation of fast crack growth in brittle solids. Int J Mech Phys Solids 42: 1397–1434

Zi G, Chen H, Xu J, Belytschko T (2005) The extended finite element method for dynamic fractures. Shock Vib 12:9–23